

Topological Thermodynamics of Generalized Bardeen Black Hole

A. A. M. Silva,^{1,*} M. H. Macêdo,^{1,†} and R. R. Landim^{1,‡}

¹*Universidade Federal do Ceará (UFC), Departamento de Física,
Campus do Pici, Fortaleza - CE, C.P. 6030, 60455-760 - Brazil.*

Neves and Saa introduced a two-parameter spacetime that includes the Hayward, Bardeen, and Simpson–Visser geometries as particular cases. In this work, we employ the generalized off-shell Helmholtz free energy method to investigate the thermodynamic properties of the generalized Bardeen black hole within a topological framework. We construct the associated vector field and analyze its zeros, whose winding numbers allow us to classify the thermodynamic branches and identify critical points associated with phase transitions. The regular black hole configurations exhibit two topological defects with opposite winding numbers, resulting in a vanishing total topological charge, while the Schwarzschild case contains a single unstable branch. Our results demonstrate how the regularization parameters affect the thermodynamic stability and phase structure of the spacetime.

I. INTRODUCTION

In 1916, Schwarzschild discovered a spherically symmetric solution to Einstein’s equations. This result was later understood as describing black holes, i.e., objects characterized by the presence of an event horizon. Since then, black holes have been confirmed by different lines of observational evidence, including the recent detections of gravitational waves by LIGO and the first images of the supermassive black hole at the center of our galaxy [1, 2]. However, the Schwarzschild solution predicts the existence of an unavoidable singularity at the center of the object. The existence of a central singularity inside a black hole is the difficulty in general relativity because physical quantities become divergent at this point, indicating that the theory is incomplete.

Sakharov and Gliner suggested that essential singularities, like the one at the center of the Schwarzschild black hole, might be avoided if the usual vacuum, with a vanishing energy–momentum tensor, were replaced by a vacuum-like medium described by a de Sitter geometry [3, 4]. Following this idea, a number of singularity-free spacetimes, known as regular solutions, were developed. Among them, Bardeen introduced a model in which the constant mass is replaced by a position-dependent function [5]. Other constructions, such as the Simpson-Visser solution, exhibit a geometry that can describe either a regular black hole or a wormhole, depending on the choice of parameters [6, 7]. Another notable regular solution was proposed by Dymnikova, based on a gravitational analogue of the Schwinger effect [8–11].

The first nonsingular black hole solution with a de Sitter core was proposed by Bardeen [12, 13]. Later, Ayón-Beato and García demonstrated that this solution can be obtained from the coupling of Einstein gravity with non-linear electrodynamic [14]. In 2006, Hayward proposed another regular solution, a static spherically symmetric black hole, with a de Sitter core [15], constructed as an effective geometry incorporating a finite curvature scale at the origin. Since then, Hayward proposal has been extended to include both charged and rotating black holes [16, 17], along with investigations of their thermodynamics and quasinormal modes [18, 19]. Both solutions describe a spacetime with a highly dense central region of de Sitter type, where $G_{\mu\nu} = -\lambda g_{\mu\nu}$ with $\lambda > 0$. Recently, a generalization of the Bardeen metric has been proposed and it can be demonstrated that the Hayward spacetime arises from this metric for a particular choice of parameters [20].

Bekenstein proposed that black holes have an entropy associated with the area of the event horizon and that their energy is connected to the black hole mass [21–23]. Later, Hawking showed that black holes can emit thermal radiation, whose temperature is related to the surface gravity of the black hole [24]. Since the interior region of a black hole cannot be directly observed, the study of thermodynamic processes outside the event horizon becomes especially relevant. In particular, one may ask how these processes change depending on whether the spacetime contains a singularity or avoids it.

The thermodynamics of regular black holes is difficult to define due to additional terms in the first law of thermodynamics, which in turn produces certain complications in establishing correspondences between mechanical and thermodynamic quantities [25]. In addition, some regular black holes do not obey the area law, $S \neq A/4$, and

* anderson.alves@fisica.ufc.br

† matheus.macedo@fisica.ufc.br

‡ renan@fisica.ufc.br

$dS = dM/T$ at the same time [26, 27]. In contrast, the thermodynamic aspect of black holes through a topological point of view has received considerable attention recently [28–32], in this approach the stability of a regular black hole can be analyzed by the topological property of the considered spacetime, thus studying the sign of the winding number allows one to verify the presence of phase transitions, changes in the sign of the heat capacity and global properties of the system [33–37].

In this work, we investigate the topological thermodynamics properties of a generalized Bardeen black hole. We compute the thermodynamic quantities, such as the Hawking temperature and heat capacity, which enables us to analyze the stability of the black hole. In addition, we employ the topological thermodynamics approach to classify the thermodynamic branches and identify possible critical points associated with phase transitions. The paper is organized as follows: In Sec. II we present the solution for the generalized Bardeen black hole. In Sec. III we discuss the topological thermodynamics associated with the black hole. Finally, we summarize the paper in Sec IV.

II. REVIEW OF GENERALIZED BARDEEN BLACK HOLE

Neves and Saa obtained a static and spherically symmetric spacetime with two classes of parameters that possesses the Bardeen, Hayward and Simpson-Visser metrics as special cases [38], which made it possible to analyze how different regularization mechanisms affect the structure of spacetime, mainly near the central region. The generalized Bardeen black hole has a line element of the form [20]

$$ds^2 = -f(r)dt^2 + \frac{dr^2}{f(r)} + r^2d\Omega^2, \quad (1)$$

where

$$f(r) = 1 - \frac{2Mr^{\alpha-1}}{(r^\beta + a^\beta)^{\alpha/\beta}}. \quad (2)$$

Here M and a are the mass and length parameters, respectively, while α and β are positive real parameters. This metric reduces to Bardeen metric when $\alpha = 3$ and $\beta = 2$, to the Hayward metric if $\alpha = \beta = 3$ and Simpson-Visser for $\alpha = 1$ and $\beta = 2$, provided that M and a are suitably identified. Furthermore, it approaches the Schwarzschild black hole in the limit $r \gg a$. If we want this metric to behave like de Sitter space for small values of r , it is necessary that $\alpha = 3$, since

$$f(r \rightarrow 0) = 1 - \frac{2Mr^{\alpha-1}}{a^\alpha} = 1 - \frac{r^2}{r_0^2}, \quad \text{where } r_0^2 = \frac{a^3}{2M}.$$

and asymptotically approaches the Schwarzschild form

$$f(r \rightarrow \infty) = 1 - \frac{2M}{r}$$

The black hole mass, as a function of the horizon radius, is obtained by setting $f(r_h) = 0$ and is equals to

$$M(r_h) = \frac{1}{2}r_h^{1-\alpha} (r_h^\beta + a^\beta)^{\alpha/\beta} \quad (3)$$

Since $M(r_h)$ decreases for $r_h < r_{ext}$ and increases for $r_h > r_{ext}$ it possesses a global minimum at $r_{ext} = a(\alpha - 1)^{1/\beta}$. Therefore, horizons exist only for $M \geq M^* = M(r_{ext})$. For $M > M^*$ the equation admits two positive roots, corresponding to the inner and outer horizons where $r_- < r_{ext} < r_+$, while for $M = M^*$ these roots coincide. The ‘‘remnant possibility’’ refers to the scenario where the Hawking temperature vanishes, indicating a remnant black hole that does not evaporate completely. The black hole remnant could serve as potential dark matter candidates, as their stability and non-evaporating nature make them viable for such a role [39–41]. For the generalized Bardeen metric, the Hawking temperature is

$$T = \frac{1}{4\pi} \frac{r_h^\beta - (\alpha - 1)a^\beta}{r_h(r_h^\beta + a^\beta)} \quad (4)$$

which vanishes at $r_h = r_{ext}$, the corresponding mass is finite and equal to $M^* = \frac{aa^{\alpha/\beta}}{2(\alpha-1)^{(\alpha-1)/\beta}}$. Therefore, the

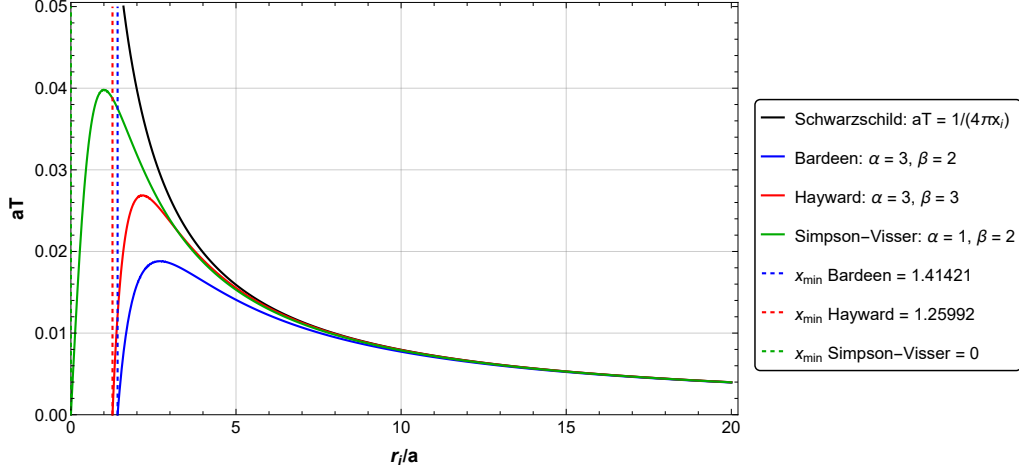


FIG. 1. Plot of aT as a function of r_i/a .

extremal configuration can be interpreted as a black hole remnant. It is worth noting that for $r \gg a$, the Hawking temperature reduces to that of a Schwarzschild black hole, while for $r \ll a$ and $\alpha = 3$ it approaches the de Sitter temperature. We present in Fig.1 a plot of the Hawking temperature as a function of the event horizon, for all parameters choices the temperature vanishes at $r_h = r_{ext}$. As r_h increases the Hawking temperature rises to a finite maximum and subsequently decreases approaching the Schwarzschild black hole at large distances.

A change in the sign of the heat capacity may indicate a possible phase transition in the black hole, whereas local stability is associated with a positive heat capacity while local instability occurs when the heat capacity is negative. The heat capacity of the generalized Bardeen black hole is given by:

$$C = \frac{2\pi r_h^{2-\alpha} (a^\beta + r_h^\beta)^{\frac{\alpha+\beta}{\beta}} [r_h^\beta - a^\beta (\alpha - 1)]}{(\alpha - 1)a^{2\beta} - r_h^{2\beta} + a^\beta r_h^\beta [\alpha(\beta + 1) - 2]} \quad (5)$$

Figure 2 displays plots of the heat capacity (5) for different values of α, β . The heat capacity has one critical point [42], being such point related to the maximum of the Hawking temperature. Hence, the critical point sets the value of r_h in which generalized Bardeen black hole exhibit a phase transition, and as we can see, the critical point is (α, β) -dependent.

The Kretschmann scalar invariant for metric (2) has the form

$$K = 4M^2 r^{2(\alpha-3)} (a^\beta + r^\beta)^{-2(2+\frac{\alpha}{\beta})} \{ 12r^{4\beta} + a^{4\beta} [12 + \alpha(-20 + \alpha(17 - 6\alpha + \alpha^2)) - 4a^\beta r^{3\beta} [-12 + \alpha(5 + \beta)] - 2a^{3\beta} r^\beta [-24 + \alpha(30 + 2\beta - 17\alpha - 3\alpha\beta + 3\alpha^2 + \alpha^2\beta) + a^{2\beta} r^{2\beta} (72 + \alpha(-60 - 8\beta + \alpha(17 + \beta(6 + \beta)))] \}. \quad (6)$$

For $\beta > 0$ and $\alpha \geq 3$ the metric is regular everywhere, including at $r = 0$. It reduces to the Schwarzschild solution in the limit $a \rightarrow 0$ and approaches the de Sitter value $\frac{24}{r_0^4}$ when $\alpha = 3$ and $r \rightarrow 0$, acting as a limiting value for the spacetime curvature. Hence, the length parameter a removes the curvature singularity which occurs in the Schwarzschild black hole.

The components of Einstein equations yield

$$\rho(r) = \frac{M\alpha a^\beta r^{\alpha-3}}{4\pi(a^\beta + r^\beta)^{\alpha/\beta+1}} = -p(r) \quad (7)$$

$$p_t = \frac{1}{8\pi} a^\beta M r^{\alpha-3} (a^\beta + r^\beta)^{-2-\alpha/\beta} [(1 + \beta)r^\beta - a^\beta (\alpha - 1)] \quad (8)$$

It is evident that the null energy condition (NEC) is valid for all r , but the strong energy condition (SEC) is violated at the center but not away from the center. Alternatively, the SEC is satisfied if $p_t \geq 0$, which occurs when $r \geq \frac{r_{ext}}{(1+\beta)^{1/\beta}}$.

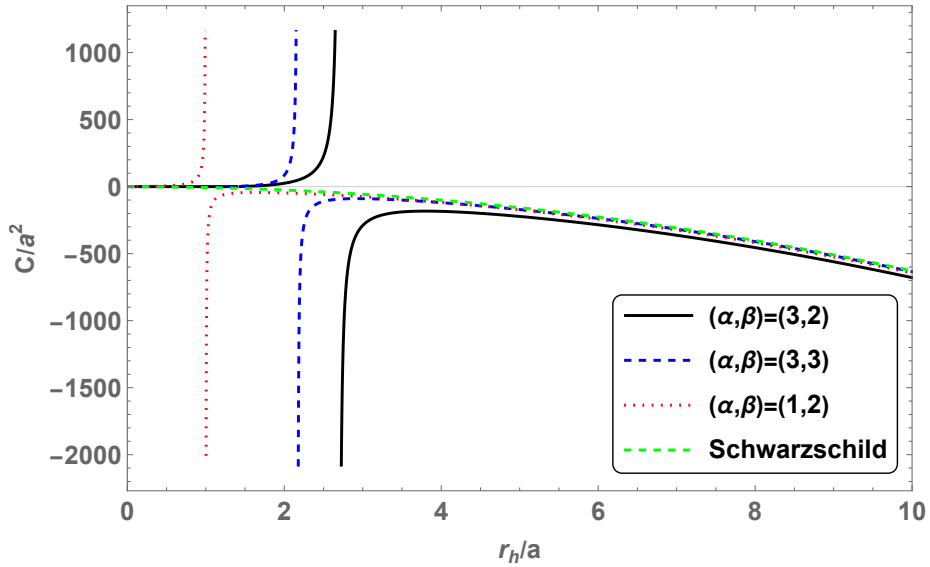


FIG. 2. Plotting the heat capacity (C) as a function of the event horizon radius (r_+) for the generalized Bardeen black hole across different parameters α and β .

III. TOPOLOGICAL THERMODYNAMIC FOR GENERALIZED BARDEEN BLACK HOLE

A. Thermodynamic Topology

1. General Case

Let us now analyze the topological features of the generalized Bardeen black hole, following Refs. [43, 44]. The black hole entropy, obtained from

$$S = \int \frac{dM}{T}, \quad (9)$$

is given by

$$S(r_h) = \frac{2\pi r_h^{2-\alpha} (a^\beta + r_h^\beta)^{\alpha/\beta} (a^{-\beta} r_h^\beta + 1)^{-\alpha/\beta} {}_2F_1\left(\frac{2-\alpha}{\beta}, -\frac{\alpha}{\beta}; \frac{2-\alpha}{\beta} + 1; -a^{-\beta} r_h^\beta\right)}{2-\alpha}, \quad (10)$$

where ${}_2F_1(a, b; c; x)$ is the hypergeometric function. With this quantity, we compute the generalized off-shell Helmholtz free energy, defined as [45, 46]

$$\mathcal{F} = M - \frac{S}{\tau}, \quad (11)$$

where τ is the Euclidean time period, satisfying $\tau = 1/T$ on shell. For the generalized Bardeen black hole, one obtains

$$\mathcal{F} = \frac{\frac{1}{2} r_h^{1-\alpha} (a^\beta + r_h^\beta)^{\alpha/\beta} - \frac{2\pi r_h^{2-\alpha} (a^\beta + r_h^\beta)^{\alpha/\beta} (a^{-\beta} r_h^\beta + 1)^{-\alpha/\beta} {}_2F_1\left(\frac{2-\alpha}{\beta}, -\frac{\alpha}{\beta}; \frac{2-\alpha}{\beta} + 1; -a^{-\beta} r_h^\beta\right)}{(2-\alpha)\tau}. \quad (12)$$

Following Ref. [13], we define the vector field

$$\vec{\phi} = \left(\frac{\partial \mathcal{F}}{\partial r_h}, -\cot \Theta \csc \Theta \right), \quad (13)$$

where $0 \leq \Theta \leq \pi$ is an auxiliary parameter. The zeros of this vector field are obtained from $\vec{\phi} = 0$. Since the second component vanishes at $\Theta = \pi/2$, the first component gives

$$\left. \frac{\partial \mathcal{F}}{\partial r_h} \right|_{r_h=r_i} = 0. \quad (14)$$

From this condition, we obtain the Euclidean time period

$$\tau = \frac{4\pi r_i (a^\beta + r_i^\beta)}{r_i^\beta + (1 - \alpha)a^\beta}. \quad (15)$$

This expression is the inverse of the Hawking temperature in Eq. (4), as expected from the on-shell relation $\tau = 1/T$ in the topological thermodynamic approach [43].

Introducing the dimensionless variable

$$y_i = \frac{r_i}{a}, \quad (16)$$

and defining $\tau^* = \tau/a$, Eq. (15) becomes

$$\tau^* = \frac{4\pi y_i (1 + y_i^\beta)}{y_i^\beta + 1 - \alpha}. \quad (17)$$

In the asymptotic regime $r_i \gg a$, one has

$$a^\beta + r_i^\beta \simeq r_i^\beta, \quad r_i^\beta + (1 - \alpha)a^\beta \simeq r_i^\beta. \quad (18)$$

Therefore, Eq. (15) reduces to

$$\tau = 4\pi r_i, \quad (19)$$

which is precisely the Schwarzschild result obtained in Ref. [43].

For the computation of the winding numbers, we proceed in a way similar to Ref. [36]. The winding number associated with each zero of the vector field is determined by

$$w_i = \text{sgn} \left[\left. \frac{\partial^2 \mathcal{F}}{\partial r_h^2} \right|_{r_h=r_i} \right], \quad (20)$$

where

$$\left. \frac{\partial^2 \mathcal{F}}{\partial r_h^2} \right|_{r_h=r_i} = r_i^{-\alpha-1} (a^\beta + r_i^\beta)^{\frac{\alpha}{\beta}-2} [(\alpha - 1)a^{2\beta} + a^\beta(\alpha\beta + \alpha - 2)r_i^\beta - r_i^{2\beta}]. \quad (21)$$

Since $r_i > 0$, $\alpha > 0$, and $\beta > 0$, the prefactor outside the square brackets is positive. Hence, the sign of the second derivative is determined only by

$$(\alpha - 1)a^{2\beta} + a^\beta(\alpha\beta + \alpha - 2)r_i^\beta - r_i^{2\beta}. \quad (22)$$

Defining

$$z_i = \left(\frac{r_i}{a} \right)^\beta, \quad (23)$$

the sign analysis reduces to the quadratic function

$$G(z_i) = (\alpha - 1) + [\alpha(\beta + 1) - 2] z_i - z_i^2. \quad (24)$$

Thus,

$$w_i = \text{sgn} [(\alpha - 1) + [\alpha(\beta + 1) - 2] z_i - z_i^2]. \quad (25)$$

The roots of $G(z_i)$ are

$$z_i = \frac{\alpha(\beta + 1) - 2 \pm \sqrt{[\alpha(\beta + 1) - 2]^2 + 4(\alpha - 1)}}{2}. \quad (26)$$

For $\alpha \geq 1$, the negative root is not physically relevant. Therefore, the only positive root is

$$z_i^* = \frac{\alpha(\beta + 1) - 2 + \sqrt{[\alpha(\beta + 1) - 2]^2 + 4(\alpha - 1)}}{2}. \quad (27)$$

Since $G(z_i)$ is a quadratic function with negative concavity, its sign is positive before the positive root and negative after it. Hence,

$$\begin{cases} G(z_i) > 0, & 0 \leq z_i < z_i^*, \\ G(z_i) = 0, & z_i = z_i^*, \\ G(z_i) < 0, & z_i > z_i^*. \end{cases} \quad (28)$$

Returning to the variable r_i/a , we define the critical radius

$$x_c \equiv \frac{r_i}{a} = \left[\frac{\alpha(\beta + 1) - 2 + \sqrt{[\alpha(\beta + 1) - 2]^2 + 4(\alpha - 1)}}{2} \right]^{1/\beta}. \quad (29)$$

Therefore, the winding numbers are classified as

$$\begin{cases} w_i = +1, & 0 \leq \frac{r_i}{a} < x_c, \\ w_i = 0, & \frac{r_i}{a} = x_c, \\ w_i = -1, & \frac{r_i}{a} > x_c. \end{cases} \quad (30)$$

It is worth emphasizing that, in this work, we distinguish between two sign functions as in [36]. The function $\text{sgn}(x)$ is defined in the extended sense,

$$\text{sgn}(x) = \begin{cases} +1, & x > 0, \\ 0, & x = 0, \\ -1, & x < 0, \end{cases} \quad (31)$$

and is used to characterize the winding numbers, which may vanish at the critical point. On the other hand, $\text{Sgn}(x)$ denotes the sign associated with the heat capacity away from the critical point, where only the values ± 1 are considered. Thus, $\text{sgn}(x) = 0$ identifies the critical configuration, while $\text{Sgn}(C) = \pm 1$ characterizes the locally stable or unstable thermodynamic branches.

Since the sign of the winding number agrees with the sign of the heat capacity, as discussed in Ref. [36], one obtains

$$\begin{cases} \text{Sgn}(C) = +1, & 0 \leq \frac{r_i}{a} < x_c, & \text{topologically stable branch,} \\ \text{Sgn}(C) = -1, & \frac{r_i}{a} > x_c, & \text{topologically unstable branch.} \end{cases} \quad (32)$$

At $w_i = 0$, or equivalently at $r_i/a = x_c$, the condition

$$M''S' - M'S'' = 0 \quad (33)$$

is satisfied. This point signals a possible phase transition and corresponds to the point where the heat capacity diverges or changes sign.

In the asymptotic regime, $r \gg a$, the generalized metric approaches the Schwarzschild limit. Since this regime corresponds to $r/a > x_c$, one obtains $w_i = -1$ and therefore $\text{Sgn}(C) = -1$, consistently with the well-known thermodynamic instability of the Schwarzschild black hole [43].

2. *Bardeen Black Hole for $\alpha = 3$ and $\beta = 2$*

We now consider the topological structure of the Bardeen black hole, obtained from the generalized metric by taking $\alpha = 3$ and $\beta = 2$. In this case, the mass as a function of the horizon radius is given by

$$M_{\text{Bardeen}} = \frac{(a^2 + r_h^2)^{3/2}}{2r_h^2}. \quad (34)$$

The corresponding Hawking temperature is

$$T_{\text{Bardeen}} = \frac{r_h^2 - 2a^2}{4\pi r_h (r_h^2 + a^2)}. \quad (35)$$

The entropy obtained from $S = \int dM/T$ reads

$$S_{\text{Bardeen}} = \frac{\pi (r_h^2 - 2a^2) \sqrt{a^2 + r_h^2}}{r_h} + 3\pi a^2 \tanh^{-1} \left(\frac{r_h}{\sqrt{a^2 + r_h^2}} \right). \quad (36)$$

These expressions are consistent with the results reported in the literature [47]. From these quantities, the generalized off-shell Helmholtz free energy is obtained as

$$\mathcal{F}_{\text{Bardeen}} = \frac{\sqrt{a^2 + r_h^2} [a^2(4\pi r_h + \tau) + r_h^2(\tau - 2\pi r_h)] - 6\pi a^2 r_h^2 \tanh^{-1} \left(\frac{r_h}{\sqrt{a^2 + r_h^2}} \right)}{2r_h^2 \tau}. \quad (37)$$

Using the vector field defined in Eq. (13), the zeros of the field are obtained by imposing

$$\left. \frac{\partial \mathcal{F}_{\text{Bardeen}}}{\partial r_h} \right|_{r_h=r_i} = 0. \quad (38)$$

This condition gives

$$\tau_{\text{Bardeen}} = \frac{4\pi r_i (a^2 + r_i^2)}{r_i^2 - 2a^2}. \quad (39)$$

Therefore, the on-shell temperature satisfies

$$T_{\text{Bardeen}} = \frac{1}{\tau_{\text{Bardeen}}}, \quad (40)$$

in agreement with Eq. (35) and with the topological thermodynamic construction [43].

For the winding numbers and the heat-capacity sign, we use the general intervals given in Eqs. (30) and (32). For $\alpha = 3$ and $\beta = 2$ in the equation (29), the critical value is

$$x_c \approx 2.697. \quad (41)$$

Thus, for the Bardeen case,

$$\begin{cases} w_i = +1, & \text{Sgn}(C) = +1, & 0 < \frac{r_i}{a} < 2.697, & \text{stable branch,} \\ w_i = 0, & & \frac{r_i}{a} = 2.697, & \text{critical point,} \\ w_i = -1, & \text{Sgn}(C) = -1, & \frac{r_i}{a} > 2.697, & \text{unstable branch.} \end{cases} \quad (42)$$

The value $r_i/a = 2.697$ corresponds to the point where the heat capacity diverges and changes sign.

3. Hayward Black Hole for $\alpha = \beta = 3$

The Hayward black hole is obtained from the generalized metric by choosing $\alpha = \beta = 3$. In this case, the mass is

$$M_{\text{Hayward}} = \frac{a^3 + r_h^3}{2r_h^2}. \quad (43)$$

The Hawking temperature is given by

$$T_{\text{Hayward}} = \frac{r_h^3 - 2a^3}{4\pi r_h (a^3 + r_h^3)}. \quad (44)$$

The entropy reads

$$S_{\text{Hayward}} = \frac{\pi (r_h^3 - 2a^3)}{r_h}. \quad (45)$$

Therefore, the generalized off-shell Helmholtz free energy becomes

$$\mathcal{F}_{\text{Hayward}} = \frac{a^3(4\pi r_h + \tau) + r_h^3(\tau - 2\pi r_h)}{2r_h^2\tau}. \quad (46)$$

The zeros of the vector field are obtained from

$$\left. \frac{\partial \mathcal{F}_{\text{Hayward}}}{\partial r_h} \right|_{r_h=r_i} = 0, \quad (47)$$

which leads to

$$\tau_{\text{Hayward}} = \frac{4\pi r_i (a^3 + r_i^3)}{r_i^3 - 2a^3}. \quad (48)$$

Once again, the on-shell relation

$$T_{\text{Hayward}} = \frac{1}{\tau_{\text{Hayward}}} \quad (49)$$

reproduces the Hawking temperature in Eq. (44), confirming the consistency of the topological approach.

For $\alpha = \beta = 3$, the critical value obtained from the general expression (29) is

$$x_c \approx 2.168. \quad (50)$$

Thus, the winding numbers and the sign of the heat capacity are classified as

$$\begin{cases} w_i = +1, & \text{Sgn}(C) = +1, & 0 < \frac{r_i}{a} < 2.168, & \text{stable branch,} \\ w_i = 0, & & \frac{r_i}{a} = 2.168, & \text{critical point,} \\ w_i = -1, & \text{Sgn}(C) = -1, & \frac{r_i}{a} > 2.168, & \text{unstable branch.} \end{cases} \quad (51)$$

As in the Bardeen case, the critical point $\frac{r_i}{a} = 2.168$ separates the locally stable and unstable thermodynamic branches.

4. Simpson-Visser Black Hole for $\alpha = 1$ and $\beta = 2$

Finally, we consider the Simpson-Visser case, obtained by setting $\alpha = 1$ and $\beta = 2$. The mass is given by

$$M_{\text{SV}} = \frac{1}{2} \sqrt{a^2 + r_h^2}. \quad (52)$$

The corresponding temperature is

$$T_{\text{SV}} = \frac{r_h}{4\pi(a^2 + r_h^2)}. \quad (53)$$

The entropy is

$$S_{\text{SV}} = \pi \left[r_h \sqrt{a^2 + r_h^2} + a^2 \tanh^{-1} \left(\frac{r_h}{\sqrt{a^2 + r_h^2}} \right) \right]. \quad (54)$$

From these quantities, the generalized off-shell Helmholtz free energy reads

$$\mathcal{F}_{\text{SV}} = \frac{1}{2} \sqrt{a^2 + r_h^2} - \frac{\pi \left[r_h \sqrt{a^2 + r_h^2} + a^2 \tanh^{-1} \left(\frac{r_h}{\sqrt{a^2 + r_h^2}} \right) \right]}{\tau}. \quad (55)$$

The condition for the zeros of the vector field,

$$\left. \frac{\partial \mathcal{F}_{\text{SV}}}{\partial r_h} \right|_{r_h=r_i} = 0, \quad (56)$$

gives

$$\tau_{\text{SV}} = \frac{4\pi(a^2 + r_i^2)}{r_i}. \quad (57)$$

Thus,

$$T_{\text{SV}} = \frac{1}{\tau_{\text{SV}}}, \quad (58)$$

which agrees with the Simpson–Visser temperature in Eq. (53).

For $\alpha = 1$ and $\beta = 2$ in (29), the critical value is

$$x_c = 1. \quad (59)$$

Therefore, the winding numbers and the heat-capacity sign are given by

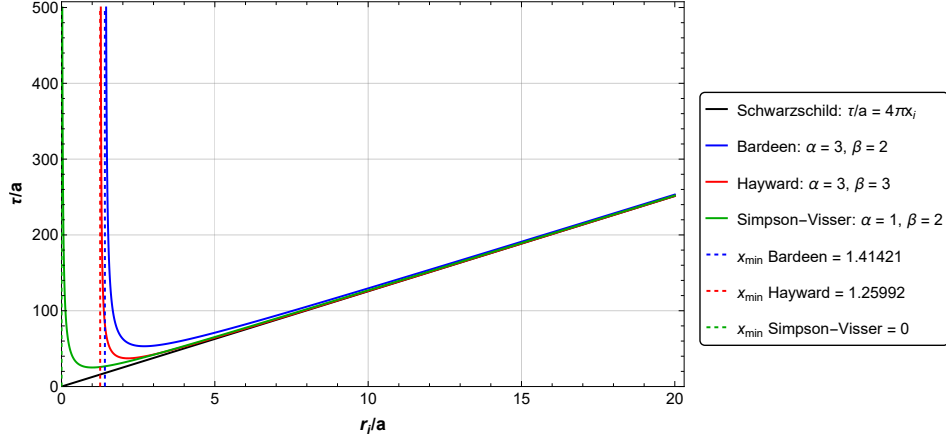
$$\begin{cases} w_i = +1, & \text{Sgn}(C) = +1, & 0 < \frac{r_i}{a} < 1, & \text{stable branch,} \\ w_i = 0, & & \frac{r_i}{a} = 1, & \text{critical point,} \\ w_i = -1, & \text{Sgn}(C) = -1, & \frac{r_i}{a} > 1, & \text{unstable branch.} \end{cases} \quad (60)$$

Hence, the Simpson–Visser geometry also exhibits a change in thermodynamic stability at the critical point $r_i/a = 1$.

IV. RESULTS AND DISCUSSION

In the previous section, the topological thermodynamics of the generalized metric given in Eq. (2) was investigated. By fixing the parameters α and β , the Bardeen, Hayward, and Simpson–Visser geometries are recovered as particular cases. Starting from the general formulation, it was possible to obtain the relevant topological quantities and to verify the consistency of the approach by recovering the Hawking temperature from the on-shell relation $\tau = 1/T$, evaluated at $r_h = r_i$. Figures 1 and 3 show, respectively, the dimensionless temperature $T^* = aT$ and the dimensionless inverse temperature $\tau^* = \tau/a$ as functions of the dimensionless horizon radius $x_i = r_i/a$.

Figure 3 shows the behavior of τ/a as a function of r_i/a . The vertical dotted lines indicate the extremal radii, given by $x_{\text{min}} = \frac{r_{\text{ext}}}{a} = (\alpha - 1)^{1/\beta}$. These values define the lower bound of the physical black-hole branch for each case. At $r_i/a = r_{\text{ext}}/a$, the Hawking temperature vanishes and, consequently, $\tau/a \rightarrow \infty$, since $\tau = 1/T$ on shell. For sufficiently large values of r_i/a , all regular cases asymptotically recover the Schwarzschild behavior.

FIG. 3. Plot of τ/a as a function of r_i/a .

Spacetime	r_i/a	τ/a
Bardeen ($\alpha = 3, \beta = 2$)	2.69721	53.1706
Hayward ($\alpha = \beta = 3$)	2.16843	37.2232
Simpson-Visser ($\alpha = 1, \beta = 2$)	1	25.1327
Schwarzschild (asymptotic case)	No critical point	No critical point

TABLE I. Critical values of τ/a as a function of r_i/a .

The critical values of τ/a for each spacetime are summarized in Table I. These critical points correspond to the points where the heat capacity diverges and changes sign. Thus, they separate locally stable and unstable thermodynamic branches. In contrast, the Schwarzschild case does not exhibit a finite critical point, since $\tau/a = 4\pi r_i/a$ is a monotonic function.

Since $T^* = aT = 1/\tau^*$, the critical values of the dimensionless temperature are the inverse of the corresponding critical values of τ/a . These values are presented in Table II. The Simpson-Visser case reaches the highest maximum temperature, followed by the Hayward and Bardeen cases. Equivalently, the minimum value of τ/a is lowest for Simpson-Visser and highest for Bardeen. This behavior shows that the parameters α and β , which encode the regularization mechanism of the spacetime, directly affect the location of the critical points and the thermodynamic stability structure.

Spacetime	r_i/a	aT
Bardeen ($\alpha = 3, \beta = 2$)	2.69721	0.0188074
Hayward ($\alpha = \beta = 3$)	2.16843	0.0268649
Simpson-Visser ($\alpha = 1, \beta = 2$)	1	0.0397887
Schwarzschild (asymptotic case)	No critical point	No critical point

TABLE II. Critical values of aT as a function of r_i/a .

To complement the analysis based on the extrema of τ/a and aT , Fig. 4 displays the normalized vector field

$$\vec{n} = \frac{\vec{\phi}}{|\vec{\phi}|}, \quad (61)$$

where

$$\vec{\phi} = \left(\frac{\partial \mathcal{F}}{\partial r_h}, -\csc \Theta \cot \Theta \right). \quad (62)$$

The zeros of this vector field occur when both components vanish simultaneously. The second component vanishes at $\Theta = \pi/2$, while the first component gives the condition $\partial \mathcal{F}/\partial r_h = 0$. Therefore, the defects appear along the line $\Theta = \pi/2$ and are associated with the values of r_i/a that satisfy the off-shell condition for a fixed value of τ .

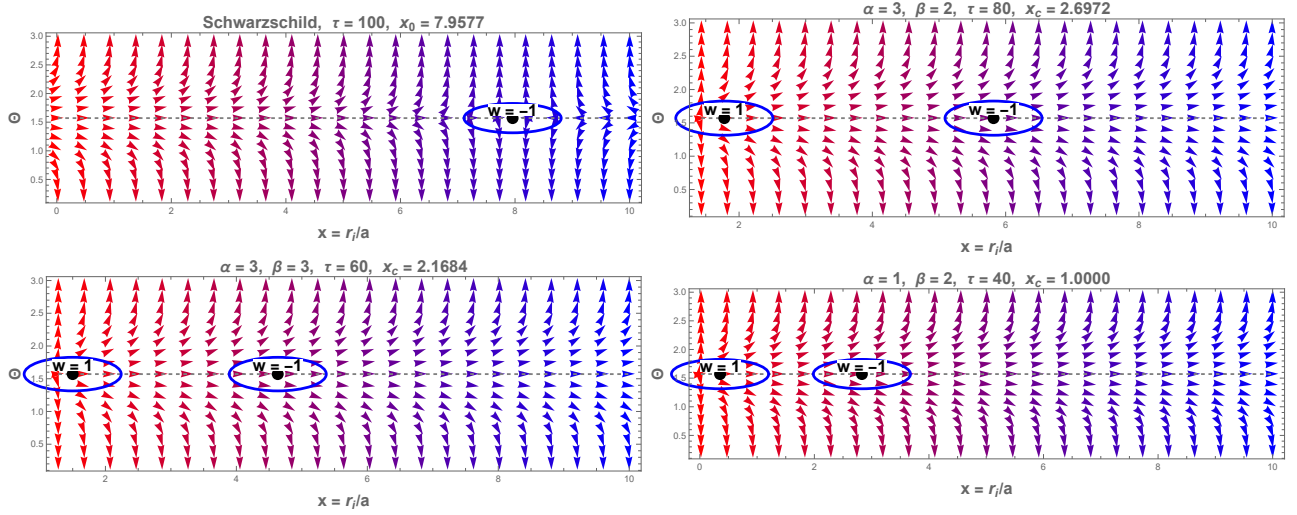


FIG. 4. Normalized vector field $\vec{n} = \vec{\phi}/|\vec{\phi}|$ for the Schwarzschild, Bardeen, Hayward, and Simpson–Visser cases. The circles indicate the zeros of the vector field, and the corresponding winding numbers are shown near each defect.

For the Schwarzschild case, the off-shell free energy leads to a single zero for a fixed value of τ . Since the heat capacity of the Schwarzschild black hole is always negative, this defect carries winding number $w = -1$, in agreement with its thermodynamic instability. This is consistent with the absence of a finite critical point in Tables I and II, because $\tau/a = 4\pi r_i/a$ is monotonic and does not present a local minimum.

For the regular cases, the behavior is different. The Bardeen, Hayward, and Simpson–Visser spacetimes exhibit two zeros of the vector field for the selected values of τ . These zeros lie on opposite sides of the critical value in equation (30)

$$x_c = \left[\frac{\alpha(\beta + 1) - 2 + \sqrt{[\alpha(\beta + 1) - 2]^2 + 4(\alpha - 1)}}{2} \right]^{1/\beta}. \quad (63)$$

According to the sign of

$$\left. \frac{\partial^2 \mathcal{F}}{\partial r_h^2} \right|_{r_h=r_i}, \quad (64)$$

the defect located in the region $r_i/a < x_c$ has winding number $w = +1$, whereas the defect located in the region $r_i/a > x_c$ has winding number $w = -1$. Thus, the first defect corresponds to a locally stable thermodynamic branch, while the second corresponds to an unstable branch.

In the Bardeen case, with $(\alpha, \beta) = (3, 2)$, the critical value is $x_c = 2.6972$. For the value $\tau = 80$ used in Fig. 4, the vector field displays two defects: one before and one after x_c . The left defect has $w = +1$, while the right defect has $w = -1$. The same qualitative structure occurs for the Hayward case, where $(\alpha, \beta) = (3, 3)$ and $x_c = 2.1684$, and for the Simpson–Visser case, where $(\alpha, \beta) = (1, 2)$ and $x_c = 1$. In all these regular cases, the two defects appear as a pair with opposite winding numbers.

Therefore, for the regular spacetimes analyzed here, the total topological charge is

$$W = \sum_i w_i = +1 - 1 = 0. \quad (65)$$

This result shows that the regular black-hole configurations considered in this work contain one stable and one unstable branch for the chosen values of τ . The transition between these branches occurs precisely at the point where the heat capacity diverges and changes sign. Consequently, the vector-field analysis gives a direct topological interpretation of the thermodynamic behavior already observed in Figs. 3 and 1.

Overall, the results confirm the consistency between the topological approach and the standard thermodynamic analysis. The zeros of the vector field reproduce the inverse Hawking temperature through the on-shell condition $\tau = 1/T$, while the sign of the winding number agrees with the sign of the heat capacity. The Schwarzschild case exhibits a single unstable defect with $w = -1$, reflecting its negative heat capacity. In contrast, the Bardeen, Hayward,

and Simpson–Visser cases exhibit pairs of defects with opposite winding numbers, $w = +1$ and $w = -1$, corresponding respectively to locally stable and unstable thermodynamic branches. Thus, the generalized Bardeen metric provides a unified framework in which different regular black holes can be compared through their topological thermodynamic structure.

V. CONCLUSION

In this work, we investigated the topological thermodynamics of the generalized Bardeen black hole through the off-shell Helmholtz free energy formalism. This geometry provides a unified framework that contains the Bardeen, Hayward, and Simpson–Visser spacetimes as particular cases, obtained by suitable choices of the parameters α and β . By analyzing the zeros of the vector field

$$\vec{\phi} = \left(\frac{\partial \mathcal{F}}{\partial r_h}, -\csc \Theta \cot \Theta \right), \quad (66)$$

we showed that the topological approach consistently reproduces the standard thermodynamic behavior of these black holes.

The condition $\partial \mathcal{F} / \partial r_h = 0$ leads to the on-shell relation $\tau = 1/T$, confirming that the zeros of the vector field are directly associated with the thermodynamic states of the black hole. In dimensionless form, the inverse temperature $\tau^* = \tau/a$ and the temperature $T^* = aT$ were analyzed for the Schwarzschild, Bardeen, Hayward, and Simpson–Visser cases. The regular black holes exhibit an extremal radius at which the Hawking temperature vanishes, while their temperature curves present a finite maximum. This maximum corresponds to the points where the heat capacity diverges and changes sign.

The winding number analysis shows that the sign of the topological charge agrees with the sign of the heat capacity. For the Bardeen, Hayward, and Simpson–Visser cases, the vector field presents two defects for the selected values of τ . The defect located before the critical point x_c has winding number $w = +1$ and corresponds to a locally stable branch, whereas the defect located after x_c has winding number $w = -1$ and corresponds to an unstable branch. Therefore, for these regular black holes, the total topological charge is

$$W = \sum_i w_i = +1 - 1 = 0. \quad (67)$$

In contrast, the Schwarzschild case exhibits only one defect with winding number $w = -1$, reflecting its negative heat capacity and thermodynamic instability. This difference highlights the effect of the regularization parameters α and β on the thermodynamic and topological structure of the spacetime. In particular, the position of the points where the thermal capacity sign changes depends explicitly on these parameters, showing that different regularization mechanisms lead to different stability domains.

Overall, our results demonstrate that the generalized Bardeen metric offers a useful setting for comparing regular black holes from a topological thermodynamic perspective. The correspondence between the winding number and the heat-capacity sign confirms the consistency between the topological and standard thermodynamic descriptions. Future investigations may extend this analysis to charged, rotating, or higher-dimensional generalizations, as well as to other regular black-hole models where additional thermodynamic variables modify the topological structure of the phase space.

ACKNOWLEDGMENTS

The authors thank the Coordenação de Aperfeiçoamento de Pessoal de Nível Superior (CAPES) and the Conselho Nacional de Desenvolvimento Científico e Tecnológico (CNPq).

-
- [1] B. P. Abbott *et al.* (LIGO Scientific, Virgo), *Phys. Rev. Lett.* **116**, 061102 (2016), arXiv:1602.03837 [gr-qc].
 - [2] K. Akiyama *et al.* (Event Horizon Telescope), *Astrophys. J. Lett.* **875**, L1 (2019), arXiv:1906.11238 [astro-ph.GA].
 - [3] A. D. Sakharov, *Soviet Journal of Experimental and Theoretical Physics* **22**, 241 (1966).
 - [4] E. B. Gliner, *Soviet Journal of Experimental and Theoretical Physics* **22**, 378 (1966).
 - [5] J. Bardeen, in *Proceedings of the 5th International Conference on Gravitation and the Theory of Relativity* (1968) p. 87.

- [6] A. Simpson and M. Visser, *JCAP* **02**, 042 (2019), arXiv:1812.07114 [gr-qc].
- [7] A. Lima, G. Alencar, and J. Furtado, “Black string bounce to traversable wormhole,” (2022), arXiv:2211.12349 [gr-qc].
- [8] M. H. Macêdo, J. Furtado, and R. R. Landim, *Eur. Phys. J. C* **86**, 57 (2026), arXiv:2507.03701 [gr-qc].
- [9] M. H. Macêdo, J. Furtado, G. Alencar, and R. R. Landim, *Annals Phys.* **471**, 169833 (2024), arXiv:2404.02818 [gr-qc].
- [10] F. Ahmed, S. Murodov, B. Rahmatov, and A. Bouzenada, (2026), arXiv:2602.22264 [gr-qc].
- [11] M. Estrada and R. Aros, *Eur. Phys. J. C* **79**, 810 (2019), arXiv:1906.01152 [gr-qc].
- [12] A. Kumar, D. Veer Singh, and S. G. Ghosh, *Eur. Phys. J. C* **79**, 275 (2019), arXiv:1808.06498 [gr-qc].
- [13] J. Sadeghi, S. Noori Gashti, M. R. Alipour, and M. A. S. Afshar, *Annals Phys.* **455**, 169391 (2023), arXiv:2306.05692 [hep-th].
- [14] E. Ayon-Beato and A. Garcia, *Phys. Lett. B* **493**, 149 (2000), arXiv:gr-qc/0009077.
- [15] S. A. Hayward, *Phys. Rev. Lett.* **96**, 031103 (2006), arXiv:gr-qc/0506126.
- [16] V. P. Frolov, *Phys. Rev. D* **94**, 104056 (2016), arXiv:1609.01758 [gr-qc].
- [17] M. Amir and S. G. Ghosh, *JHEP* **07**, 015 (2015), arXiv:1503.08553 [gr-qc].
- [18] M. Molina and J. R. Villanueva, *Class. Quant. Grav.* **38**, 105002 (2021), arXiv:2101.07917 [gr-qc].
- [19] K. Lin, J. Li, and S. Yang, *Int. J. Theor. Phys.* **52**, 3771 (2013).
- [20] P. Dutta Roy and S. Kar, *Phys. Rev. D* **106**, 044028 (2022), arXiv:2206.04505 [gr-qc].
- [21] J. D. Bekenstein, *Lett. Nuovo Cim.* **4**, 737 (1972).
- [22] J. D. Bekenstein, *Phys. Rev. D* **7**, 2333 (1973).
- [23] J. D. Bekenstein, *Phys. Rev. D* **7**, 2333 (1973).
- [24] S. W. Hawking, *Communications in Mathematical Physics* **43**, 199 (1975).
- [25] Y. Zhang and S. Gao, *Class. Quant. Grav.* **35**, 145007 (2018), arXiv:1610.01237 [gr-qc].
- [26] C. Lan, H. Yang, Y. Guo, and Y.-G. Miao, *Int. J. Theor. Phys.* **62**, 202 (2023), arXiv:2303.11696 [gr-qc].
- [27] C. Lan, Y.-G. Miao, and H. Yang, *Nucl. Phys. B* **971**, 115539 (2021), arXiv:2008.04609 [gr-qc].
- [28] M. Shahzad, N. Alessa, A. Mehmood, and R. Javed, *Astronomy and Computing* **51**, 100900 (2025).
- [29] B. Hazarika and P. Phukon, *Nucl. Phys. B* **1006**, 116649 (2024), arXiv:2312.06324 [hep-th].
- [30] S.-X. Bao, Z.-J. Wan, and Y.-Z. Du, *Communications in Theoretical Physics* **78**, 015402 (2025).
- [31] Y. Sekhmani, S. Maurya, J. Rayimbaev, M. Altanji, I. Ibragimov, and S. Muminov, *Physics of the Dark Universe* **50**, 102079 (2025).
- [32] G. Nashed and M. Bedair, *Physics Letters B* **869**, 139866 (2025).
- [33] S.-W. Wei, Y.-X. Liu, and R. B. Mann, *Phys. Rev. Lett.* **123**, 071103 (2019), arXiv:1906.10840 [gr-qc].
- [34] S.-W. Wei and Y.-X. Liu, *Phys. Rev. D* **105**, 104003 (2022), arXiv:2112.01706 [gr-qc].
- [35] M.-Y. Zhang, H.-Y. Zhou, H. Chen, H. Hassanabadi, and Z.-W. Long, *Eur. Phys. J. C* **85**, 1322 (2025), arXiv:2507.14439 [gr-qc].
- [36] A. A. M. Silva, G. Alencar, C. R. Muniz, M. Nilton, and R. R. Landim, “Topological thermodynamics of black holes: Revisiting the methods of winding numbers calculation,” (2025), arXiv:2511.06579 [gr-qc].
- [37] S.-P. Wu, S.-J. Yang, and S.-W. Wei, *Eur. Phys. J. C* **85**, 1372 (2025), arXiv:2508.01614 [hep-th].
- [38] J. C. S. Neves and A. Saa, *Phys. Lett. B* **734**, 44 (2014), arXiv:1402.2694 [gr-qc].
- [39] P. Chen and R. J. Adler, *Nucl. Phys. B Proc. Suppl.* **124**, 103 (2003), arXiv:gr-qc/0205106.
- [40] I. Dymnikova and M. Korpusik, *Phys. Lett. B* **685**, 12 (2010).
- [41] R. J. Adler, P. Chen, and D. I. Santiago, *Gen. Rel. Grav.* **33**, 2101 (2001), arXiv:gr-qc/0106080.
- [42] P. C. W. Davies, *Class. Quant. Grav.* **6**, 1909 (1989).
- [43] S.-W. Wei, Y.-X. Liu, and R. B. Mann, *Phys. Rev. Lett.* **129**, 191101 (2022), arXiv:2208.01932 [gr-qc].
- [44] S.-W. Wei, Y.-X. Liu, and R. B. Mann, *Phys. Rev. D* **110**, L081501 (2024), arXiv:2409.09333 [gr-qc].
- [45] D. Wu, *Phys. Rev. D* **107**, 024024 (2023), arXiv:2211.15151 [gr-qc].
- [46] D. Wu and S.-Q. Wu, *Phys. Rev. D* **107**, 084002 (2023), arXiv:2301.03002 [hep-th].
- [47] M. Sharif and W. Javed, *J. Korean Phys. Soc.* **57**, 217 (2010), arXiv:1007.4995 [gr-qc].